A. Ozgurluk, R. Liu, and C. T.-C. Nguyen, "Q-boosting of metal MEMS resonators via localized anneal-induced tensile stress," *Proceedings*, IEEE Int. Frequency Control Symp., Besancon, France, July 10-13, 2017, pp. 10-15, DOI: 10.1109/FCS.2017.8088786.

Q-Boosting of Metal MEMS Resonators Via Localized Anneal-Induced Tensile Stress

Alper Ozgurluk, Ruonan Liu, and Clark T.-C. Nguyen

Dept. of Electrical Engineering and Computer Sciences
University of California at Berkeley
Berkeley, California, USA
ozgurluk@eecs.berkeley.edu

***Abstract*— Introduction of tensile stress via localized Joule heating has yielded some of the highest metal MEMS resonator *Q*'s measured to date, as high as 48,919 for a 12-MHz ruthenium micromechanical clamped-clamped beam ('CC-beam'). The high *Q*'s continue into the VHF range, with *Q*'s of 7,202 and 4,904 at 61 and 70 MHz, respectively. These marks are substantially higher than the 6,000 at 10 MHz and 300 at 70 MHz previously measured for polysilicon CC-beams, defying the common belief that metal *Q* cannot compete with conventional micromachinable materials. The low-temperature ruthenium metal process, with highest temperature of 450°C and paths to an even lower ceiling of 200°C, further allows for MEMS post-processing directly over finished foundry CMOS wafers, thereby offering a promising route towards fully monolithic realization of CMOS-MEMS circuits, such as needed in communication transceivers. This, together with its higher *Q*, may eventually make ruthenium metal preferable over polysilicon in some applications.**

Keywords*— *MEMS, micromechanical resonator, ruthenium, localized annealing, quality factor, tensile stress, integration

I. Introduction

Oscillators referenced to high-Q micromechanical resonators that consume only 78 μW of power while attaining GSM-compliant phase noise performance have emerged as potential enablers for future low power autonomous wireless networks [1]. Although impressive, the bond-wired two-chip approach to realizing these MEMS-based oscillators inevitably incurs parasitic bond pad capacitances on the order of picofarads, thereby preventing these oscillators from realizing their true potential for power consumption [1]. Here, single-chip CMOS-MEMS integration to remove bond pad capacitance poses a nice solution. To date, however, high deposition temperatures for polysilicon or diamond MEMS materials hinder progress towards MEMS-last single chip integration alongside transistors. Their high structural and interconnect resistances also complicate applications that demand low loss, such as front-end filters. Structural and interconnect resistance also compromises MEMS-last integration approaches using SiGe structural material, which otherwise would meet temperature ceiling requirements for previous generation CMOS [2].

Ultimately, resistance needs might best be met by metal structural material options, many of which provide the added advantage of much lower deposition temperature making them more amenable to MEMS-last integration with CMOS. Unfortunately, to date metals post much lower Q's than polysilicon, SiGe, or diamond counterparts [3]. If a metal is to replace these materials, some method is needed to enhance its Q without requiring transistor-damaging temperatures.

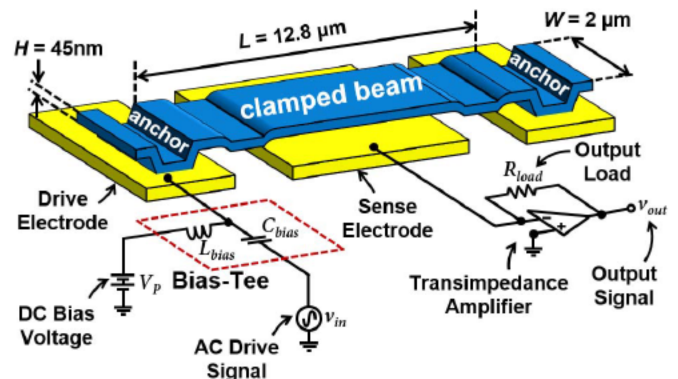

Fig. 1: Illustration of a single-electrode clamped-clamed (CC-beam) in a typical bias/excitation configuration.

Even without the draw of transistor-MEMS integration, there are burgeoning opportunities to apply high-Q metal structural material towards new all-mechanical circuits capable of detecting and demodulating RF signals while consuming no power when listening for inputs [4]. Such circuits can potentially obviate conventional sleep/wake methods intended to minimize sensor network power and in the process eliminate the clocks and computational overhead on which they rely. Here, the sensitivity, i.e., minimum detectable power, of such a circuit goes as the inverse of the Q of the resonator portion of the resoswitch they employ [4], which yet again, calls for a method for Q enhancement.

This paper demonstrates one such method that very effectively employs localized annealing to induce tensile stress in ruthenium clamped-clamped beam ('CC-beam') resonators and thereby raise their Q's through mechanisms similar to those seen for nitride resonators [5], but with orders of magnitude lower thermal exposure for underlying transistors. Use of this method yields ruthenium resonator Q's as high as 48,919 at frequencies approaching 12 MHz (to be compared with Q ~6,000 for polysilicon [6]); and retains high Q at VHF as indicated by Q's of 7,202 and 4,904 at 61 and 70 MHz,

respectively (to be compared with Q ~300 at 70 MHz for polysilicon [7]).

II. Device Structure and Operation

Fig. 1 summarizes the CC-beam micromechanical resonator device [6] used as a vehicle in this work in a typical bias, excitation, and evaluation circuit. The CC-beam differs from previous renditions [6] in not only the material used, which is now Ru; but also in its dimensions, which are substantially smaller than previous ones in order to maximize sensitivity for a resoswitch-based receiver application [4]. Specifically, unlike previous polysilicon CC-beam dimensions on the order of of 40.8µm-long, 8µm-wide, and 1.9µm-thick to reach 7.81 MHz, a typical Ru design herein is 12.8µm-long, 2µm-wide, and 45 nm-thick, with dimensions 3.2, 4, and 42 times smaller, respectively. This reduces the mass and stiffness needed to achieve a given frequency, which improves (i.e., minimizes) sensitivity P_{sens} according to

$$P_{sens} = \frac{d_o^2 k_m \omega_0}{Q} \quad (1)$$

where k_m, d_o, and ω_0 are the mechanical stiffness, switch gap, and resonance frequency of the resoswitch, respectively. Note that smaller stiffness improves sensitivity, i.e., makes it smaller, by not only the direct stiffness term k_m in the numerator of (1), but also by reducing anchor dissipation, thereby raising the Q term in the denominator.

With Q as a focus, the devices herein were tested as resonators, rather than resoswitches, using the circuit of Fig. 1. Here, the bias-tee-combined AC-DC voltages of the drive and bias inputs together generate an amplified force at the frequency of the AC signal across the input-electrode-to-resonator gap. Sweeping the frequency of the AC source around the beam's resonance frequency generates vibrational motion that in turn creates a DC-biased time-varying capacitance across the electrode-to-resonator gap. A current then ensues, flowing through the structure and gap, out of the center electrode, and into the awaiting transimpedance amplifier detector.

As mentioned, this work boosts Q by introducing tension into the CC-beam. Of course, this tension affects not only Q, but also the resonance frequency. With tension added, the resonance frequency expression for the CC-beam becomes

$$f_0 = 1.03 \frac{H}{L^2} \sqrt{\frac{E}{\rho}} \sqrt{1 + \frac{SL^2}{3.4EH^2}} \quad (2)$$

where f_0 is resonant frequency, E is Young's modulus, ρ is density, S is tensile stress, and Fig. 1 identifies geometric parameters.

III. Fabrication

The choice of ruthenium as a metal for this work has more to do with the fact that its oxide is also conductive, making it useful for resoswitches [8] as well as resonators. The process used to achieve the device of Fig. 1 employs a surface micromachining process that uses Ru for interconnect, low-

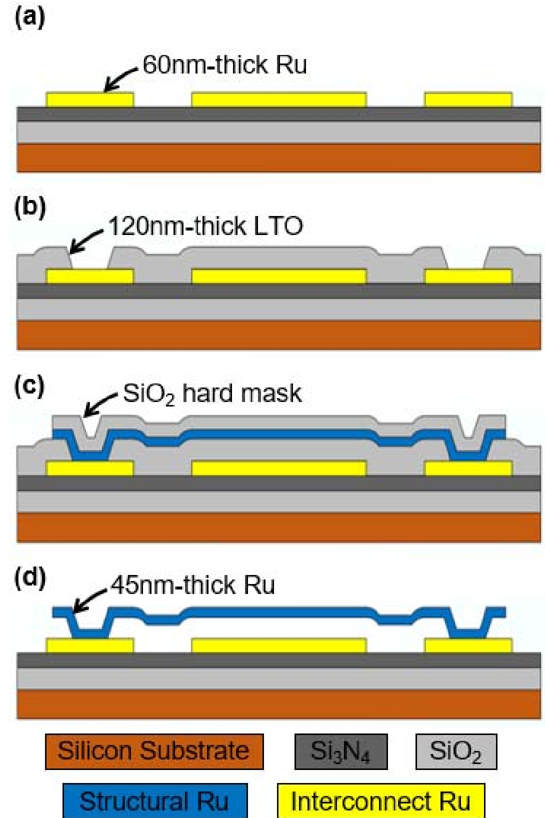

Fig. 2: Cross-sections describing the ruthenium metal CC-beam fabrication process flow after (a) patterning ruthenium interconnect and removing its etch hard mask; (b) depositing sacrificial layer and etching anchor openings; (c) depositing and patterning structural ruthenium; and (d) releasing the structure in HF.

temperature LPCVD oxide as a sacrificial layer, and sputtered Ru (only 45 nm-thick) as the structural material. Fig. 2 summarizes the fabrication process.

The fabrication starts on 6″ blank p-type Si wafers with successive LPCVD depositions of 2µm LTO and 500nm silicon rich nitride at 450ºC and 835ºC, respectively, to serve as electrical isolation layers. Note that the silicon nitride could be replaced by a lower temperature material, such as alumina, if this process were actually run over CMOS, which it presently is not. Sputtering of 60nm-thick Ru and PECVD deposition at 350ºC of 60nm-thick thick oxide then follow to serve as the interconnect layer and the oxide hard mask used in its etching, respectively. Lithography via a first mask and dry etch using Ar:CHF_3:CF_4 then transfers the interconnect layer pattern into the oxide hard mask. Next, a dry etch with Applied Materials Centura DPS etcher using gas flow rates of 90sccm of O_2 and 20sccm of Cl_2 at 20mTorr pressure with source and bias powers of 300W and 50W, respectively, delineates the interconnect layer as depicted in Fig. 2(a); followed by a 1 minute 5:1 buffered HF dip to remove the oxide hard mask layer.

Note that the need for a hard mask when etching the interconnect layer is not a consequence of the etch selectivity of the Ru dry etch chemistry over photoresist, which is actually quite adequate. Rather, it derives from a need to avoid cross-linking between Ru and photoresist observed at elevated temperatures [9]. In particular, even without hard- or UV-baking,

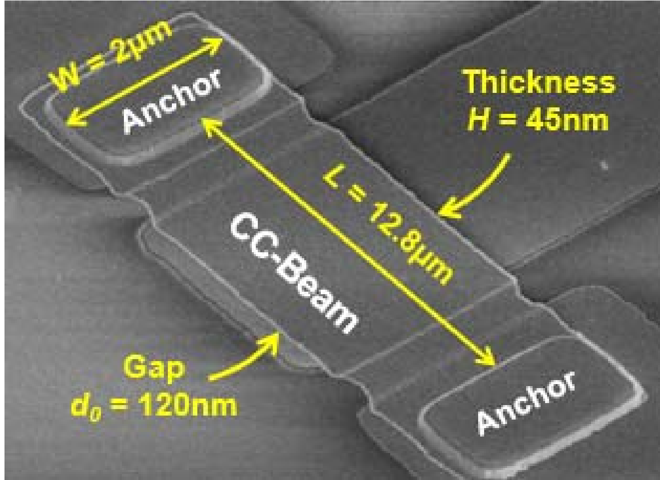

Fig. 3: SEM of a fabricated CC-beam resonator with key dimensions.

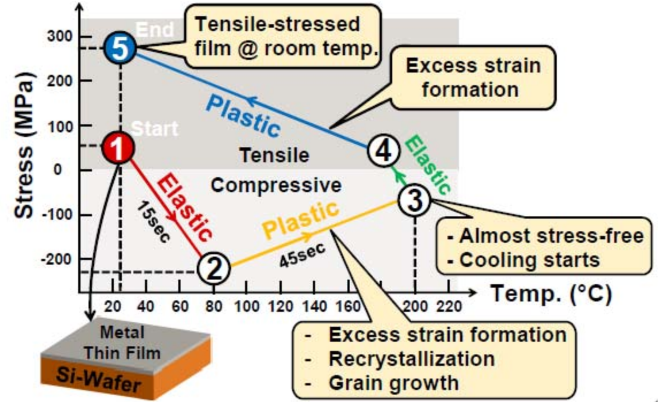

Fig. 4: A generic thermal annealing cycle for low-temperature sputtered metals atop Si substrate showing how film stress evolves during heating and cooling.

the temperature elevation that occurs during dry etching of Ru is enough to instigate cross-linking so strong that removal of photoresist after Ru layer patterning becomes very difficult.

After interconnect layer patterning, LPCVD deposition of low temperature oxide (LTO) at 450°C coats a sacrificial oxide layer that defines the 120nm capacitive actuation gap between the CC-beam and the underlying electrode. Anchor openings are then etched into the oxide sacrificial layer using Ar:CHF_3:CF_4 as illustrated in Fig. 2(b), followed by a sputtering of 45nm Ru to serve as the structural material. After depositing and patterning another oxide hard mask, the same chemistry that etched the interconnect layer delineates the structures as in Fig. 2(c). Here, a Ru etch chemistry comprised of mostly O_2 with a small amount of etch-rate enhancing Cl_2 provides good selectivity (> 10) over the underlying sacrificial LTO layer [9]. This degree of selectivity becomes ever more critical for beam type devices with very small actuation gaps, i.e. < 20nm, intended for highly sensitive resoswitches.

Completed wafers are diced and the resulting dies released (when needed) in 49 wt. % liquid HF that frees the resonators. Since the small size and stiffness of the devices make them more prone to stiction, criticial point drying (CPD) is generally needed after HF release to insure adequate yield. Fig. 2(d) presents the final cross-section of the device. Fig. 3 presents the SEM of a fabricated 12.8μm-long device.

IV. TENSILE-STRESSED RUTHENIUM CC-BEAMS

As shown in Fig. 5(a), immediately after fabrication, beams with dimensions shown in Fig. 1 post frequencies around 1.2 MHz with Q's on the order of only 180, which is quite low. These represent the nearly stress-free performance of the devices, or at least the performance before stress introduction.

Again, the strategy behind the present work is to introduce stress in order to attain higher Q. If previous work with nitride resonators holds [5], better Q should be possible via introduction of tensile stress. This previous work introduced stress mechanically, by tightening a pull system via turns of a screw.

Before presenting the localized anneal-based approach to tensile stress introduction that facilitates MEMS-last integration with transistors, we first confirm and gauge the degree to which tensile stress raises the Q's Ru CC-beams via rapid thermal annealing (RTA). Here, ruthenium CC-beams of different sizes were subjected to various rapid thermal anneals (RTAs) that generated tensile stress by stimulating structure reorganization and grain growth via plastic deformation [10], [11].

To better convey how tensile stress might ensue after an anneal cycle, Fig. 4 presents a plot of stress as a function of temperature and time during annealing and cooling periods. Initially, assuming the structural material thermal expansion coefficient is larger than that of the substrate, as the temperature rises the beam strain is predominantly elastic and compressive. When the temperature surpasses a certain value, a combination of excessive compressive strain and temperature induce recrystallization, which grows grains to relieve the stress, actually reduces the compressive stress and brings the total stress closer to zero at the end of the heating cycle.

When heating stops, the cooling process begins. Now the structure, with its relatively larger thermal expansion coefficient, shrinks faster than the substrate. Since the stress at the start of the cooling process was considerably smaller than if no recrystallization had occurred, very little of the beam shrinking during cooling goes towards compensation of compressive stress, so the beam goes into heavy tension. Tension values on the order of 700-900 MPa are typical in this work.

Using (2), curve fitting measured frequency versus beam length curves as in Fig. 6 yields the following values for material parameters: Young's modulus, E = 402.5 GPa and density ρ =13,420 kg/m^3.

Note that for large values of stress, (2) reduces to

$$f_0 \cong \frac{0.56}{L}\sqrt{\frac{S}{\rho}} \quad if \;\; S \gg 3.4E\left(\frac{H}{L}\right)^2 \tag{3}$$

Here, the stress S becomes a principal determinant of resonance frequency. While on the one hand, some might argue

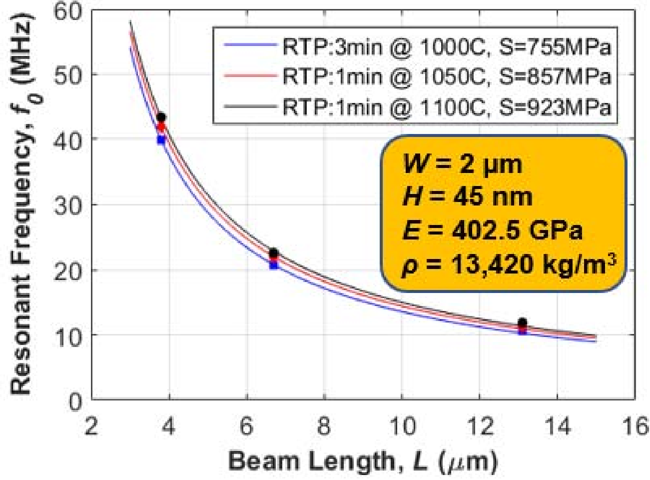

Fig. 6: Curve fitting measured frequency versus beam length where dots represent actual measured data and solid lines are analytically determined curves using (2).

that the frequency stability becomes too dependent on factors that might change the stress; others on the other hand might argue that this strong dependence on stress removes concern for instabilities in other parameters, such as Young's modulus and thickness. Ultimately, if the resonance frequency stability depends only on stress, then this might actually simplify strategies to maximize the stability of an oscillator referenced to this device, since one now need only find a method to stabilize stress. Yes, a tall order, but perhaps not an impossible one.

The dominance of stress as a determinant in (3) also suppresses the influence of non-idealities on resonance frequency. This can greatly facilitate design. For example, for the beams measured in this work, the large stress obviates the beam topography factor that would otherwise reduce the resonance frequency of a CC-beam from the theoretically expected value.

Returning to the influence of stress on Q, Table I documents the increase in frequency and Q experienced by beams

TABLE I. MEASURED Q'S AND RESONANT FREQUENCIES FOR CC-BEAMS OF DIFFERENT LENGTHS AFTER VARIOUS RTA CONDITIONS

Beam Length	Q and f_0 in Various RTA Conditions		
	1000°C, 3 min *S = 755 MPa*	*1050°C, 1 min* *S = 857 MPa*	*1100°C, 1 min* *S = 923 MPa*
L = 12.8 µm	Q = 8,617 f_0 = 10.5 MHz	Q = 9,872 f_0 = 11.3 MHz	Q = 46,066 f_0 = 11.7 MHz
L = 6.4 µm	Q = 6,210 f_0 = 20.5 MHz	Q = 7,652 f_0 = 21.7 MHz	Q = 16,040 f_0 =22.5 MHz
L = 3.5 µm	Q = 1,803 f_0 = 38.2 MHz	Q = 2,576 f_0 = 39.8 MHz	Q = 5,562 f_0 = 42.9 MHz

of different lengths under various amounts of RTA-induced tensile stress. As shown, introduction of tensile stress raises the frequency of the Fig. 5(a) device by almost 10 times. In addition, 923 MPa tensile stress provides an impressive 256 times increase in Q, taking the Q of the Fig. 5(a) device from 180 to 46,066!

V. LOCALIZED ANNEALING

Although the results of Table I are quite compelling, the RTA temperatures used therein could unfortunately degrade foundry CMOS transistors. This work circumvents this problem via use of localized Joule-heating, first demonstrated in [12], that raises only the MEMS resonator device to the needed stress-inducing temperature, keeping any underlying transistors near room temperature. Here, the circuit of Fig. 5(b) simply applies a voltage V_{ann} across the beam anchors, which then sends a current I_{ann} through the beam that Joule heats it to a desired temperature, generating tensile stress in the process. The tiny size of the device presents a correspondingly tiny thermal capacitance, allowing the beam to be heated to over 1000ºC in milliseconds, which in turn allows fast pulsed annealing for more precise stress control.

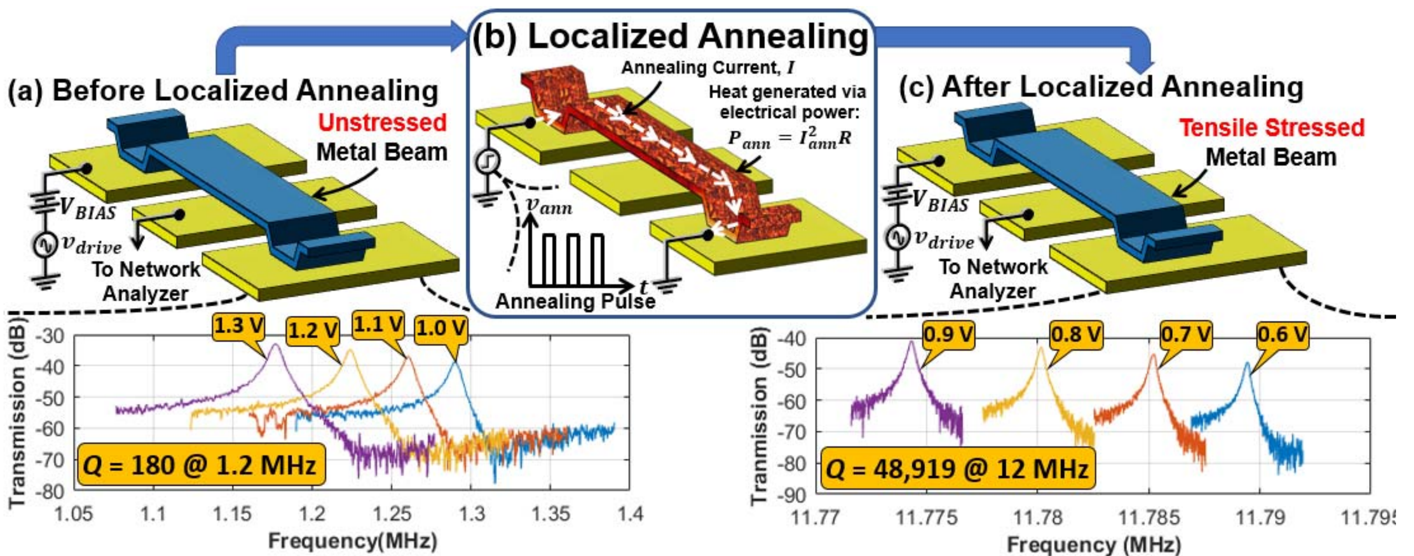

Fig. 5: Measured frequency response vs. DC bias voltage for a 12.8µm-long, 2µm-wide, 45nm-thick Ru CC-beam (a) before and (c) after localized anneal-stressing. (b) Schematic depicting the circuit needed for localized anneal-stressing.

VI. LOCALIZED ANNEAL-INDUCED Q-BOOSTING

Localized annealing experiments took advantage of the fast heating time constants characteristic at the micro-scale by heating via pulsed voltage train sequences, as shown in Fig. 7(a), which were applied across the beam annealing terminals. Here, (V_{ann}, τ_d, τ_b) sets describe specific pulse train types, where τ_d is pulse duration, and τ_b is spacing between pulses. A frequency response measurement to extract the resonance frequency and Q followed each pulse or pulse-train anneal step.

The measurement procedure was such that each device experienced successively stronger annealing each time it survived an anneal step. Specifically, if a device survives a first anneal set, the next anneal set raised the ante by either raising V_{ann} or adding pulses. This procedure continued until either excessive Joule heating destroys the beam or tensile stress breaks the beam or damages its anchors.

Fig. 5(c) presents frequency characteristics after localized anneal-induced stressing for a ruthenium metal CC-beam resonator with L = 12.8 µm, W = 2 µm, and H = 45 nm at various DC bias voltages. Here, the previous 1.2 MHz resonance frequency now approaches 12 MHz with a Q of 48,919 more than 272 times higher than the previous 180. Clearly, localized anneal-stressing is a game-changer for Ru metal CC-beams.

Fig. 7(b) gauges the efficacy of localized anneal-stressing as a function of resonator frequency by plotting measured Q versus frequency. As expected, an obvious drop in Q with increasing frequency occurs due to larger anchor loss at higher frequencies. Nevertheless, because these metal resonators are considerably thinner than previous CC-beam designs, their Q's remain high at higher frequencies, on the order of 7,202 and 4,904 at 61 and 70 MHz, respectively. These are considerably higher than the 300 typically measured for 2 µm-thick 70-MHz polysilicon CC-beams.

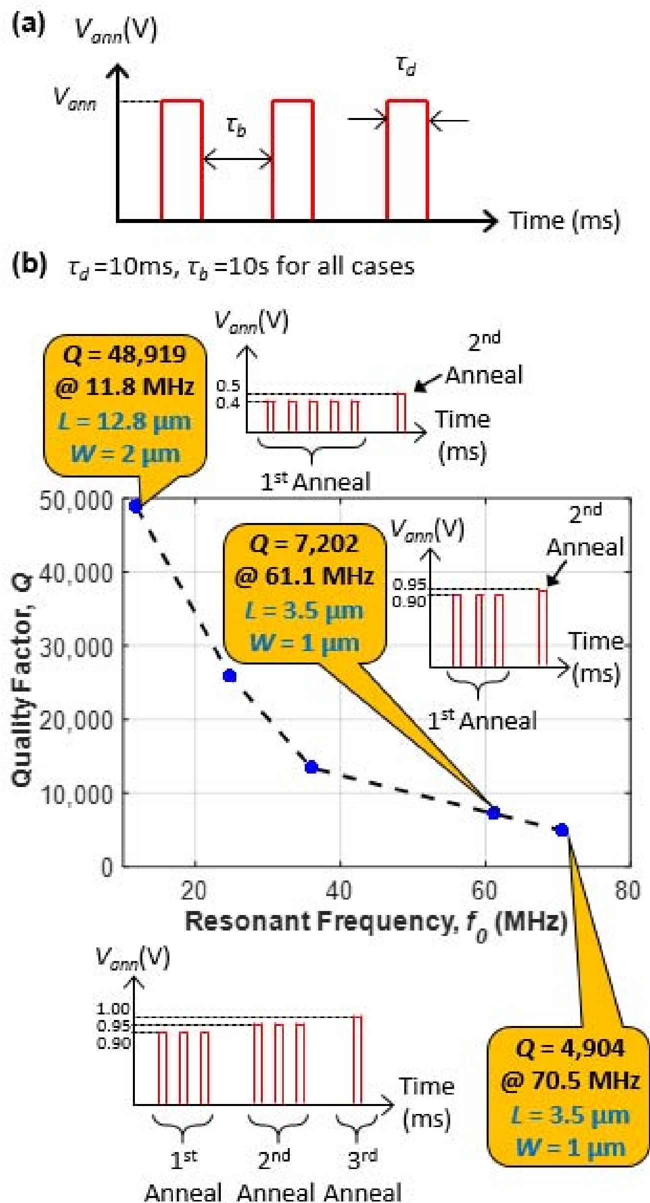

Fig. 7: (a) Pulse train localized annealing waveform used in this study. (b) Q after localized anneal-stressing as a function of beam frequency along with the localized annealing pulse conditions for certain frequencies.

VII. CONCLUSIONS

By posting Q's of 48,919 at 11.8 MHz and 4,904 at 70 MHz, both many times higher than the 6,000 and 300 typical of 2 µm-thick polysilicon counterparts, the 45 nm-thick localized anneal-stressed ruthenium metal resonators demonstrated herein may soon enable oscillators with considerably better phase noise than achieved with previous polysilicon CC-beams. Although methods to insure adequate long-term stability, e.g., via alloying, still require exploration, the results reported herein certainly enhance the feasibility of MEMS-last CMOS-MEMS integration using metal structural material.

ACKNOWLEDGMENT

This work was supported by DARPA N-ZERO program

REFERENCES

[1] T. L. Naing, T. O. Rocheleau, E. Alon, and C. T.-C. Nguyen, "A 78-microwatt GSM phase noise-compliant pierce oscillator referenced to a 61-MHz wine-glass disk resonator," in *Proc. Joint IEEE Int. Frequency Control Symp. and European Freqeuency and Time Forum*, 2013, pp. 562–565.

[2] A. E. Franke, J. M. Heck, T.-J. King, and R. T. Howe, "Polycrystalline silicon-germanium films for integrated microsystems," *J. Microelectromech. Syst.*, vol. 12, no. 2, pp. 160–171, 2003.

[3] W.-L. Huang, Z. Ren, Y.-W. Lin, H.-Y. Chen, J. Lahann, and C. T.-C. Nguyen, "Fully monolithic CMOS nickel micromechanical resonator oscillator," in *Proc. 21st IEEE International Conference on Micro Electro Mechanical Systems (MEMS)*, 2008, pp. 10–13.

[4] R. Liu, J. N. Nilchi, Y. Lin, T. L. Naing, and C. T.-C. Nguyen, "Zero Quiescent Power VLF Micromechanical Communication Receiver," in *Dig. Tech. Papers 18th Int.*

Conf. Solid-State Sens., Actuators Microsyst. (TRANSDUCERS), 2015, pp. 129–132.

[5] S. S. Verbridge, J. M. Parpia, R. B. Reichenbach, L. M. Bellan, and H. G. Craighead, "High quality factor resonance at room temperature with nanostrings under high tensile stress," *J. Appl. Phys.*, vol. 99, no. 12, pp. 1–8, 2006.

[6] F. D. Bannon, J. R. Clark, and C. T.-C. Nguyen, "High- Q HF Microelectromechanical Filters," *IEEE J. Solid-State Circuits*, vol. 35, no. 4, pp. 512–526, 2000.

[7] K. Wang, A.-C. Wong, and C. T.-C. Nguyen, "VHF Free – Free Beam High-Q Micromechanical Resonators," *J. Microelectromech. Syst.*, vol. 9, no. 3, pp. 347–360, 2000.

[8] Y. Lin, R. Liu, W.-C. Li, M. Akgul, and C. T.-C. Nguyen, "A Micromechanical Resonant Charge Pump," in *Dig. Tech. Papers 17th Int. Conf. Solid-State Sens., Actuators Microsyst. (TRANSDUCERS)*, 2013, pp. 1727–1730.

[9] I.-R. Chen, "Novel Material Integration for Reliable and Energy-Efficient NEM Relay Technology.", Ph.D. dissertation, EECS, Univ. California, Berkeley, Tech. Rep. UCB/EECS-2014-227, 2014.

[10] P. A. Flinn, D. S. Gardner, and W. D. Nix, "Measurement and Interpretation of Stress in Aluminum-Based Metallization as a Function of Thermal History," *IEEE Trans. Electron Devices*, vol. ED-34, no. 3, pp. 689–699, 1987.

[11] T. C. Hodge, S. A. Bidstrup-Allen, and P. A. Kohl, "Stresses in thin film metallization," *IEEE Trans. Compon. Packag. Manuf. Technol. A*, vol. 20, no. 2, pp. 241–250, 1997.

[12] K. Wang, A.-C. Wong, W.-T. Hsu, and C. T.-C. Nguyen, "Frequency trimming and Q-factor enhancement of micromechanical resonators via localized filament annealing," in *Dig. Tech. Papers 9th Int. Conf. Solid-State Sens., Actuators Microsyst. (TRANSDUCERS)*, 1997, vol. 1, pp. 109–112.